

RESEARCH ARTICLE SUMMARY

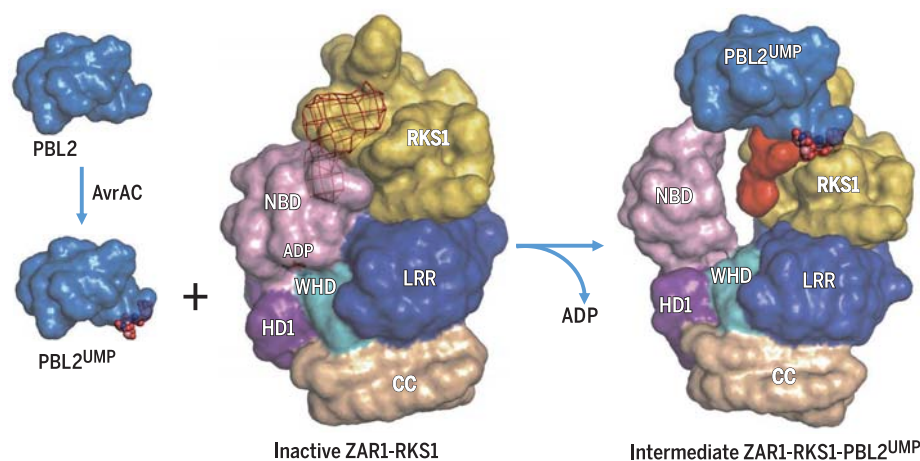
PLANT SCIENCE

Ligand-triggered allosteric ADP release primes a plant NLR complex

Jizong Wang*, Jia Wang*, Meijuan Hu*, Shan Wu, Jinfeng Qi, Guoxun Wang, Zhifu Han, Yijun Qi, Ning Gao, Hong-Wei Wang†, Jian-Min Zhou†, Jijie Chai†

INTRODUCTION: Nucleotide-binding (NB), leucine-rich repeat (LRR) receptor (NLR) proteins constitute a family of intracellular immune receptors in both animals and plants that detect the presence of pathogen molecules or host-derived signals. NLRs share a conserved tripartite domain structure with a conserved central NB and oligomerization domain (NOD), a C-terminal LRR domain, and a variable N-terminal domain. The NOD module can be further divided into an NB domain (NBD), a helical domain (HD1), and a winged-helix domain (WHD). In plants, direct or indirect recognition of pathogen effectors by NLRs induces numerous defenses, including programmed cell death called hypersensitive response, and restricts pathogens to the infection site. For instance, the coiled-coil (CC)-NLR HOPZ-ACTIVATED RESISTANCE 1 (ZARI) of the small mustard plant *Arabidopsis thaliana* forms a preactivation complex with resistance-

related kinase 1 (RKS1, a pseudokinase belonging to receptor-like cytoplasmic kinase subfamily XII-2) and recognizes the uridylyltransferase effector AvrAC from the pathogen *Xanthomonas campestris* pv. *campestris* that is responsible for the black rot disease of crucifers. AvrAC uridylylates a number of host protein kinases, including the PBS1-like protein 2 (PBL2) kinase. PBL2^{UMP}, the version of the *Arabidopsis* protein uridylylated by AvrAC, then acts as a ligand of the preformed ZARI-RKS1 complex. NLRs are believed to function as a nucleotide [adenosine diphosphate (ADP) or adenosine triphosphate (ATP)]-operated molecular switch, with ADP- and ATP-bound forms corresponding to the “off” and “on” states, respectively, but the mechanism of how ADP is released from an NLR for exchange with ATP remains elusive. Structural elucidation of a full-length plant NLR protein and its recognition of modified self is lacking.



PBL2^{UMP}-induced ADP release from ZARI. ZARI is maintained in an inactive state through contacts of multiple domains and an ADP molecule (in stick representation). ZARI^{LRR} mediates ZARI interaction with RKS1. The AvrAC-uridylylated PBL2 (PBL2^{UMP}, blue) as a ligand is exclusively recognized by the ZARI-bound RKS1. The activation segment of RKS1, which is flexible in the inactive ZARI-RKS1 complex (red mesh), becomes stabilized (red surface) after interaction with the two uridylyl moieties (in sphere representation) of PBL2^{UMP} and clashes with ZARI^{NBD}. The steric interference then causes ZARI^{NBD} to rotate outward and, consequently, ADP release. The ZARI-RKS1-PBL2^{UMP} complex thus represents an intermediate state.

RATIONALE: We reconstituted a ZARI-RKS1 and a ZARI-RKS1-PBL2^{UMP} complex and determined their cryo-electron microscopy (cryo-EM) structures at resolutions of 3.7 and 4.3 Å, respectively. The structures were verified by biochemical, cell-based, and functional data. We determined how PBL2^{UMP} affects the ADP-binding activity of the ZARI-RKS1 complex by radiolabeled assays.

ON OUR WEBSITE

Read the full article at <http://dx.doi.org/10.1126/science.aav5868>

Structural comparison of the ZARI-RKS1 and ZARI-RKS1-PBL2^{UMP} complexes was used to probe the mechanism of PBL2^{UMP}-induced ADP release from ZARI, which was further validated by biochemical assays.

RESULTS: The cryo-EM structure of the ZARI-RKS1 complex revealed that intramolecular interactions within ZARI maintain the NLR protein in an inactive state. The inactive state is further stabilized by an ADP. The LRR domain of ZARI (ZARI^{LRR}) is positioned differently from LRR domains of animal NLRs but functions similarly to sequester ZARI in a monomeric state. ZARI^{CC} appears to be kept in an inactive state via contacts with ZARI^{LRR}, ZARI^{HD1}, and ZARI^{WHD}. This contrasts with the flexible N-terminal domain of inactive apoptotic protease-activating factor 1 (Apaf-1). ZARI^{LRR} mediates interaction with RKS1 in the preformed ZARI-RKS1 complex. The ZARI-RKS1-PBL2^{UMP} structure shows that RKS1 is exclusively responsible for the binding of PBL2^{UMP}. The two uridylyl moieties of PBL2^{UMP} interact with and consequently stabilize the activation segment of RKS1. Comparison of the two cryo-EM structures shows that the stabilized activation segment of RKS1 sterically clashes with the ADP-bound ZARI^{NBD} from the ZARI-RKS1 complex, resulting in conformational changes in the NBD but not other domains of ZARI: ZARI^{NBD} is rotated outward about 60° compared with that from the inactive ZARI. Thus, PBL2^{UMP} allosterically induces release of ADP from the ZARI-RKS1-PBL2^{UMP} complex. Indeed, radiolabeling assays showed that PBL2^{UMP}, but not PBL2, reduced the ADP-binding activity of the ZARI-RKS1 complex.

CONCLUSION: Our study revealed the mechanisms of PBL2^{UMP} recognition by ZARI-RKS1 and PBL2^{UMP}-induced priming of ZARI, providing a structural template for understanding NLR proteins. ■

The list of author affiliations is available in the full article online.

*These authors contributed equally to this work.

†Corresponding author. Email: chaijj@tsinghua.edu.cn (J.C.); jmzhou@genetics.ac.cn (J.-M.Z.); hongweiwang@tsinghua.edu.cn (H.-W.W.)

Cite this article as J. Wang et al., *Science* **364**, eaav5868 (2019). DOI: [10.1126/science.aav5868](https://doi.org/10.1126/science.aav5868)

RESEARCH ARTICLE

PLANT SCIENCE

Ligand-triggered allosteric ADP release primes a plant NLR complex

Jizong Wang^{1,2*}, Jia Wang^{2*}, Meijuan Hu^{1*}, Shan Wu², Jinfeng Qi¹, Guoxun Wang¹, Zhifu Han², Yijun Qi², Ning Gao^{2†}, Hong-Wei Wang^{2‡}, Jian-Min Zhou^{1‡}, Jijie Chai^{2,3,4‡}

Pathogen recognition by nucleotide-binding (NB), leucine-rich repeat (LRR) receptors (NLRs) plays roles in plant immunity. The *Xanthomonas campestris* pv. *campestris* effector AvrAC uridylylates the *Arabidopsis* PBL2 kinase, and the latter (PBL2^{UMP}) acts as a ligand to activate the NLR ZAR1 precomplexed with the RKS1 pseudokinase. Here we report the cryo-electron microscopy structures of ZAR1-RKS1 and ZAR1-RKS1-PBL2^{UMP} in an inactive and intermediate state, respectively. The ZAR1^{LRR} domain, compared with animal NLR^{LRR} domains, is differently positioned to sequester ZAR1 in an inactive state. Recognition of PBL2^{UMP} is exclusively through RKS1, which interacts with ZAR1^{LRR}. PBL2^{UMP} binding stabilizes the RKS1 activation segment, which sterically blocks ZAR1 adenosine diphosphate (ADP) binding. This engenders a more flexible NB domain without conformational changes in the other ZAR1 domains. Our study provides a structural template for understanding plant NLRs.

Perception of microbial pathogens by immune receptors activates plant defense responses. Whereas cell surface-localized immune receptors perceive extracellular molecular patterns associated with pathogenesis (1, 2), cytoplasmic immune receptors directly or indirectly perceive pathogen effectors that are secreted into the cytosol of plant cells (3, 4). The latter class of immune receptors are primarily nucleotide-binding (NB), leucine-rich repeat (LRR) receptors (NLRs), which constitute the majority of plant disease resistance (R) proteins. NLRs are shared by both plants and animals and are characterized by a conserved central NB and oligomerization domain (NOD), a C-terminal LRR domain, and a variable N-terminal domain (5). NOD is related to AAA+ adenosine triphosphatases (ATPases), which are defined by the structurally conserved adenosine diphosphate or adenosine triphosphate (ADP or ATP) binding motif and belong to the signal-transducing ATPase with numerous domains (STAND) subfamily, including the pro-apoptotic proteins Apaf-1 and CED-4 (6). NOD in plant NLRs is thus referred to as NB-ARC for the shared sequence in Apaf-1, R, and CED-4 proteins. Depending on their N termini, plant NLR proteins are classified into two ma-

major categories: coiled coil (CC)-NLRs and Toll interleukin-1 receptor (TIR)-NLRs (5). Activation of plant NLRs typically leads to an array of immune responses, including hypersensitive response (HR), a form of programmed cell death believed to limit pathogens to the infection site (7).

During the past two decades, efforts have been made toward understanding the mechanisms of action of plant NLRs (8). However, the proposed models of plant NLR action concerning autoinhibition, ligand recognition, and activation are largely inferred from structures of Apaf-1 and animal NLRs. On the basis of NOD in Apaf-1 (9–11) and animal NLRs (12–15), NB-ARC of plant NLRs is believed to function as a molecular switch with ADP- and ATP-bound forms dictating the “off” and “on” states of NLR signaling (16–18), respectively, but the underlying mechanism remains enigmatic. Intramolecular interactions such as the interaction between the CC domain and NB-ARC-LRR act to keep the CC-NLR protein Rx in an inactive state (19). Evidence from several studies supports a role of the C-terminal LRR domain in the perception of effectors (20–25). Direct or indirect recognition of an effector is thought to trigger conformational changes in the LRR domain, relieving its inhibition, enabling exchange of ADP for ATP, and consequently activating the NLR protein (3, 4, 8).

The *Arabidopsis* CC-NLR HOPZ-ACTIVATED RESISTANCE 1 (ZAR1) indirectly recognizes three unrelated bacterial effector proteins, all through an association with closely related pseudokinases ZED1 (26), resistance-related kinase 1 (RKS1) (27), and ZRK3 (28) that belong to receptor-like cytoplasmic kinase subfamily XII-2 (RLCK XII-2). Thus, the ZAR1-ZED1, ZAR1-RKS1, and ZAR1-ZRK3 complexes perceive the *Pseudomonas syringae* effector protein HopZ1a (26), an acetyl transferase;

the *Xanthomonas campestris* pv. *campestris* effector AvrAC (27), a uridylyl transferase; and the *P. syringae* effector HopF2 (28), a ribosyl transferase, respectively. ZAR1 is an ancient NLR that is also present in *Nicotiana benthamiana* (29). A recent study shows that *N. benthamiana* ZAR1 (NbZAR1) associates with another RLCK XII member, JIM2, to recognize the *X. campestris* *perforans* effector XopJ4, an acetyl transferase distantly related to HopZ1a (30). AvrAC uridylylates receptor-like cytoplasmic kinases belonging to family VII (RLCK-VII), including PBS1-like protein 2 (PBL2) and BIK1. BIK1 is a true virulence target of AvrAC, which is a key component of immune signaling pathways governed by transmembrane receptor kinases, and the uridylylation by AvrAC inhibits its kinase activity and dampens host defenses that are otherwise activated by BIK1. By contrast, PBL2 is a decoy which, upon uridylylation by AvrAC (referred to as PBL2^{UMP}), is recruited to the ZAR1-RKS1 complex through a direct interaction with RKS1 to trigger ZAR1 activation and disease resistance. Thus PBL2^{UMP}, a modified self, is the ligand triggering ZAR1 activation (27). Therefore, ZAR1 represents a model not only for studying indirect recognition of effectors by NLRs but also for understanding how an NLR expands its recognition specificity by association with multiple “adapter” proteins.

To understand the mechanisms of plant NLR autoinhibition and activation, we sought to solve the cryo-electron microscopy (cryo-EM) structures of the inactive ZAR1-RKS1 and intermediate ZAR1-RKS1-PBL2^{UMP} complexes. Supported by biochemical and functional data, the structures revealed extensive intramolecular interactions within ZAR1 that are further stabilized by ADP to maintain ZAR1 in an inactive state. The LRR domain plays a key role in the autoinhibition of ZAR1 and mediates the interaction with RKS1. Recognition of PBL2^{UMP} is exclusively mediated by RKS1 from the preformed ZAR1-RKS1 complex. Structural comparison revealed that PBL2^{UMP} binding allosterically facilitates ADP release from inactive ZAR1 by inducing conformational changes in the NB domain (NBD), which likely results in a nucleotide-depleted ZAR1. ZAR1 from the ZAR1-RKS1-PBL2^{UMP} complex, however, is monomeric and assumes a conformation similar to that of the inactive ZAR1 except NBD, suggesting that the monomeric ZAR1-RKS1-PBL2^{UMP} complex is in an intermediate state. Taken together, our data unveil the mechanisms of autoinhibition and AvrAC-induced nucleotide exchange of ZAR1 and suggest the existence of a second signal required for activation of the NLR protein.

Results Autoinhibition of ZAR1

To probe the autoinhibition mechanism of ZAR1, His-SUMO-tagged RKS1 was coexpressed with the full-length ZAR1 in insect cells. Pull-down and gel filtration assays showed that these two proteins strongly interacted with each other when coexpressed (fig. S1, A and B). The protein complex thus purified was then used for structural analysis with cryo-EM. After three-dimensional

¹State Key Laboratory of Plant Genomics, Institute of Genetics and Developmental Biology, Academy of Seed Design, Chinese Academy of Sciences, 100101 Beijing, China. ²Beijing Advanced Innovation Center for Structural Biology, Tsinghua-Peking Joint Center for Life Sciences, Center for Plant Biology, School of Life Sciences, Tsinghua University, 100084 Beijing, China. ³Max Planck Institute for Plant Breeding Research, D-50829 Cologne, Germany. ⁴Institute of Biochemistry, University of Cologne, Zulpicher Str. 47, 50674 Cologne, Germany.

*These authors contributed equally to this work. †Present address: School of Life Sciences, Peking University, 100871 Beijing, China. ‡Corresponding author. Email: chajij@tsinghua.edu.cn (J.C.); jmzhou@genetics.ac.cn (J.-M.Z.); hongweiwang@tsinghua.edu.cn (H.-W.W.)

(3D) classification, a subset of 148,718 particles was used for image reconstruction, generating a map with a global resolution of 3.7 Å (Fig. 1A and fig. S1, C to F) as determined with a gold-standard Fourier shell correlation.

The RKS1-bound ZAR1 contains an NB-ARC module, including a canonical NBD (ZAR1^{NBD}, residues 145 to 317), a helical domain 1 (ZAR1^{HD1}, residues 318 to 394), and a winged-helix domain (ZAR1^{WHD}, residues 395 to 514) (Fig. 1B, left, and table S1). The three structural domains of ZAR1 are similarly positioned to those of the inactive NLRC4 (Fig. 1B, right) and Apaf-1 (fig. S2A), indicating that the structure of ZAR1 represents an inactive state. This conclusion is consistent with the monomeric ZAR1-RKS1 complex protein indicated by gel filtration (fig. S1B). Compared with NOD in the inactive NLRC4, however, ZAR1^{NB-ARC} varies in packing against the other domains. The LRR domain sequesters NLRC4 in a monomeric state through structural coupling with the opposite side of the NBD where the WHD packs (Fig. 1B, right). Similar positioning of the C-terminal WD40 repeats (W, Trp; D, Asp) is also found in the inactive Apaf-1 (fig. S2A). In stark contrast, ZAR1^{WHD} interacts extensively with one lateral side of the LRR domain (ZAR1^{LRR}; Fig. 1B, left), presenting both ZAR1^{WHD} and ZAR1^{LRR} on the same side of ZAR1^{NBD}. The oligomerization of NLRC4 (13, 14), Apaf-1 (10), and other AAA+ ATPases (31, 32) is mediated by stacking of one side of the NBD of one protomer against the opposite side of the NBD of the other protomer in a lateral dimer. Structural superposition of the inactive ZAR1 (Fig. 1B, left) with a protomer from one lateral Apaf-1 (Fig. 1B, bottom), NLRC4, or CED-4 (fig. S2B) dimer suggested that such a dorsal-ventral stacking of NBDs is completely blocked by ZAR1^{LRR} in the inactive state. Thus, ZAR1^{LRR} can also play a role in sequestering ZAR1 in a monomeric state, although differently positioned compared with NLRC4^{LRR}.

In further support of the inactive conformation of the RKS1-bound ZAR1, an ADP molecule is well defined by the 3D reconstruction of the ZAR1-RKS1 complex (Fig. 1C). Like that in the inactive NLRC4 (12) and Apaf-1 (9, 11), the ADP in the inactive ZAR1 also binds the joint interface formed by ZAR1^{HD1}, ZAR1^{NBD}, and ZAR1^{WHD} via multiple polar interactions and van der Waals contacts (Fig. 1C). An inhibitory role of the WHD-ADP interaction formed between His⁴⁴³ and the β -phosphate group of ADP was demonstrated in NLRC4 activation in cell-based assays and auto-inflammatory diseases (33, 34). A similar WHD-ADP interaction in the inactive ZAR1 is also established through a hydrogen bond between His⁴⁸⁸ and the β -phosphate group of the ZAR1-bound ADP (Fig. 1C). ZAR1^{His488} corresponds to “H” of the “MHD” motif that is highly conserved among plant NLRs, and mutations of this residue result in constitutive activation of plant NLRs in several instances (17, 35, 36). These data suggest that the WHD-ADP interaction can also have an inhibitory role in ZAR1 regulation.

ZAR1^{CC} forms a four-helix bundle that is similar to the structures of the CC domains of the

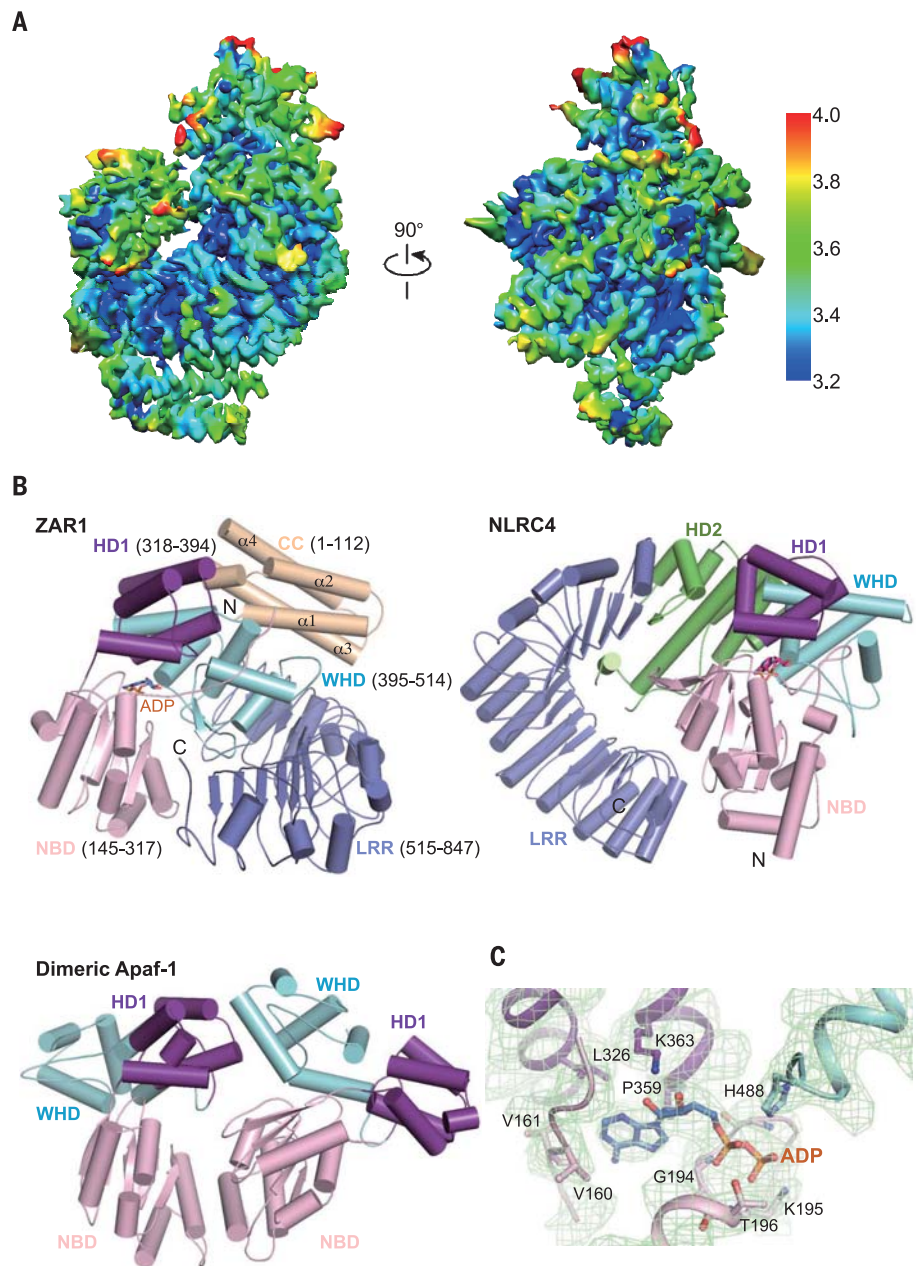


Fig. 1. Structure of inactive ZAR1. (A) Two orientations of the final EM density map of the ZAR1-RKS1 complex color coded to show the local resolution in angstroms. (B) The autoinhibition mechanisms of ZAR1, NLRC4, and Apaf-1. Shown on the top left is a cartoon representation of ZAR1 from ZAR1-RKS1. Subdomains of ZAR1 are shown in different colors, and their boundaries are indicated by residue numbers in parentheses. ADP is shown in stick representation. Shown on the top right is the structure of the inactive NLRC4 [Protein Data Bank (PDB) 4KXF] with its NBD and HD1 aligned with those of ZAR1 (top left). HD2, helical domain 2; C, C terminus; N, N terminus. Shown at the bottom left is a lateral dimer of Apaf-1 from the Apaf-1 apoptosome (PDB 3JBT). HD1 and NBD from the left protomer of the lateral dimer were aligned with those from ZAR1 (top left). (C) Binding of ADP by ZAR1. Residues of ZAR1 involved in the interaction with ADP are shown in stick representation. Cryo-EM density around the ADP binding site is shown in green mesh. Single-letter abbreviations for the amino acid residues are as follows: A, Ala; C, Cys; D, Asp; E, Glu; F, Phe; G, Gly; H, His; I, Ile; K, Lys; L, Leu; M, Met; N, Asn; P, Pro; Q, Gln; R, Arg; S, Ser; T, Thr; V, Val; W, Trp; and Y, Tyr.

CC-NLRs Rx (37) and Sr33 (38) (fig. S3). In addition to ZAR1^{LRR}, ZAR1^{CC} also packs against ZAR1^{HD1} and ZAR1^{WHD} (Fig. 1B, left). This is consistent with a previous study showing that RPM1^{CC} interacts with multiple domains of RPM1

(39). The intramolecular interactions within ZAR1 may in turn keep ZAR1^{CC} in an inactive state. This conclusion is consistent with the observation that overexpression of ZAR1^{CC}, but not ZAR1^{CC-NBD}, induces HR in plants (29). The simultaneous

interactions of ZAR1^{WHD} with the other domains result in a WHD-organized overall structure of the inactive ZAR1. ZAR1^{WHD} is therefore much more buried as compared with that in the inactive NLRC4 or Apaf-1 (Fig. 1B and fig. S2A). ZAR1^{WHD} is further buried by the N-terminal loop region of ZAR1^{NBD}, which interacts with the interface between ZAR1^{WHD} and ZAR1^{IHD} on one side (Fig. 1B, left). These intramolecular interactions collectively act to further stabilize the LRR-sequestered inactive conformation of ZAR1.

Interaction of RKS1 with ZAR1

The ZAR1-RKS1 interaction is mainly mediated by contacts of RKS1 with one lateral side of

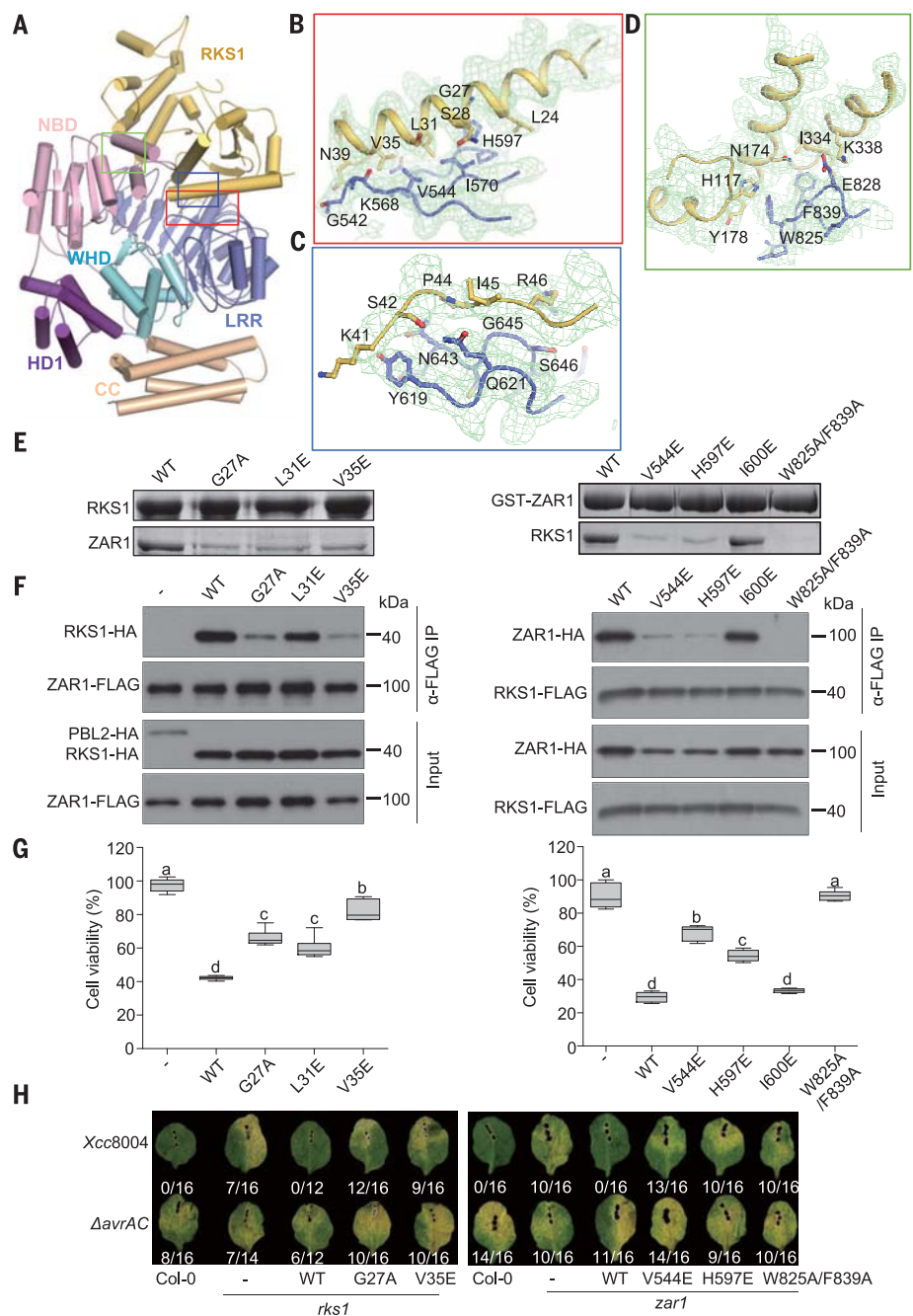
ZAR1^{LRR} (Fig. 2A). The long N-terminal α helix of RKS1 tightly packs against ZAR1^{LRR} mainly through hydrophobic contacts (Fig. 2B). In the middle of the ZAR1-RKS1 interface is the loop region C-terminal to the long α helix of RKS1, which makes polar and hydrophobic interactions with ZAR1 (Fig. 2C). At the distal side of the ZAR1-RKS1 interface, two α helices from the C-lobe of RKS1 pack against the very C-terminal side of ZAR1 via hydrophobic and van der Waals contacts (Fig. 2D). Sequence alignment indicates that the ZAR1-interacting residues of RKS1 are highly conserved among pseudokinases ZED1, ZRK3, and RKS1 and other members of the XII-2 subfamily (fig. S4). This result provides an expla-

nation for the observations that ZAR1 formed complexes with these three pseudokinases as well as other members of this RLCK subfamily (27).

Supporting our structural observations, deletion of the last LRR (29 amino acids) that interacts with the C-lobe of RKS1 (Fig. 2D) abrogated ZAR1 interaction with ZED1 (27, 29). Although not directly involved in interaction with RKS1, the ZAR1^{P816L} and ZAR1^{S831F} mutations (P816L, Pro⁸¹⁶→Leu; S831F, Ser⁸³¹→Phe) can perturb the conformation of the last LRR repeat, resulting in loss of ZAR1 interaction with RKS1 (27). The ZAR1^{G645E} mutation (Gly⁶⁴⁵→Glu) predicted to disrupt the middle ZAR1-RKS1 interface (Fig. 2C) is known to abolish ZAR1-ZED1 interaction,

Fig. 2. The C-terminal LRR domain mediates ZAR1 interaction with RKS1.

(A) Cartoon showing the overall structure of the ZAR1-RKS1 complex. The interacting regions between the two proteins are highlighted with open frames. **(B)** Detailed interactions of the N-terminal helix of RKS1 with ZAR1^{LRR} for the red-framed region in (A). Cryo-EM density is shown in green mesh. **(C)** Detailed interactions of a loop region of RKS1 with ZAR1^{LRR} for the blue-framed region in (A). **(D)** Detailed interactions of RKS1 with the last LRR of ZAR1 for the green-framed region in (A). **(E)** RKS1 (left) or ZAR1 (right) mutations reduce ZAR1-RKS1 interaction in vitro. N-terminal 6×His-SUMO tagged RKS1 was coexpressed with full-length ZAR1 (left) or glutathione S-transferase (GST)-tagged ZAR1 was coexpressed with full-length RKS1 (right) in Sf21 insect cells. The proteins were purified using Ni-NTA or glutathione sepharose 4B (GS4B) beads, and the proteins were visualized by SDS-polyacrylamide gel electrophoresis (PAGE) with Coomassie brilliant blue staining. **(F)** RKS1 (left) or ZAR1 (right) mutations diminish ZAR1-RKS1 interaction in protoplasts. Co-IP was performed using agarose-conjugated anti-FLAG (α -FLAG) antibodies, and the resulting protein was subjected to Western blot analysis. The experiments were repeated three times with similar results. HA, hemagglutinin tag; -, transfected ZAR1 construct alone as control. **(G)** RKS1 (left) or ZAR1 (right) mutations impair AvrAC-induced cell death in protoplasts. Protoplasts of *rks1* (left) or *zar1* (right) background were transfected with the indicated constructs, and a protoplast viability assay was performed. Data are represented as mean \pm SEM ($n = 6$). Different letters indicate significant difference ($P < 0.05$, Tukey post hoc test). The experiments were performed three times with similar results. -, mock control. **(H)** RKS1 (left) or ZAR1 (right) mutations abolish *avrAC*-specified disease resistance in *Arabidopsis* plants. Plants of *rks1* (left) or *zar1* (right) background complemented with the indicated constructs were inoculated with WT strain (*Xcc8004*) or a strain lacking *avrAC* (Δ *avrAC*). Disease symptoms were scored 7 days after inoculation. Numbers indicate the ratio of leaves developing chlorosis to the total number of inoculated leaves. The experiments were repeated twice with similar results. -, *rks1* and *zar1* control plants.



HopZ1a-induced HR, and disease resistance to *P. syringae* (29). To further verify our structural observations, we first introduced amino acid substitutions in RKS1 and ZARI and evaluated their impact on ZARI-RKS1 interaction using coexpression and pull-down assays. As predicted by the structure (Fig. 2, B to D), the RKS1 G27A (Gly²⁷→Ala), L31E (Leu³¹→Glu), and V35E (Val³⁵→Glu) mutations greatly impaired ZARI-RKS1 interaction in pull-down and coimmunoprecipitation (co-IP) assays (Fig. 2, E and F, and fig. S5). Similarly, the ZARI V544E (Val⁵⁴⁴→Glu), H597E (His⁵⁹⁷→Glu), and W825A/F839A (Trp⁸²⁵→Ala/Phe⁸³⁹→Ala) mutations severely diminished or abolished ZARI-RKS1 interaction in both pull-down and co-IP assays (Fig. 2, E and F, and fig. S5). The bulkier and negatively charged glutamic acid residue is more effective than an alanine residue in damaging the middle ZARI-RKS1 interface (Fig. 2C), explaining the more pronounced effect generated by ZARI^{G645E} on ZARI-ZED1 interaction (29).

We then investigated the effect of RKS1 or ZARI mutations on AvrAC-induced cell death in *Arabidopsis* protoplasts. As expected, coexpression of AvrAC with PBL2, RKS1, and ZARI in protoplasts led to cell death (Fig. 2G). By contrast, when the RKS1 or ZARI mutants with reduced ZARI-RKS1 interaction were used for the assays, the cell death activity was substantially reduced, albeit to varied degrees. To further test the observed interactions, we introduced the *RKS1* and *ZARI* variants as transgenes under control of their native promoters into *rks1* and *zar1* mutant plants, respectively. Transgenic plants of the T1 generation were inoculated with the wild-type (WT) *X. campestris* pv. *campestris* (Xcc8004), which carries functional *avrAC* and a strain lacking *avrAC* (Δ *avrAC*). As expected, the WT Col-0 plants, *rks1* plants complemented with WT *RKS1*, and *zar1* plants complemented with WT *ZARI* all displayed complete resistance to Xcc8004 and showed no chlorotic disease symptoms (Fig. 2H and fig. S6). This resistance is dependent on the recognition of AvrAC, because the Δ *avrAC* mutant strain caused disease on all genotypes. By contrast, the *RKS1*^{G27A} and *RKS1*^{V35E} variants failed to complement the *rks1* mutation, and the *ZARI*^{V544E}, *ZARI*^{H597E}, and *ZARI*^{W825A/F839A} variants failed to complement the *zar1* mutation. These transgenic plants were completely susceptible to Xcc8004 and indistinguishable from non-transgenic (-) *rks1* and *zar1* plants (Fig. 2H and fig. S6). Taken together, our biochemical and functional data support the ZARI-RKS1 interaction observed in the structure.

Structure of the ZARI-RKS1-PBL2^{UMP} complex

To understand how PBL2^{UMP} binding to RKS1 activates ZARI, we first reconstituted an RKS1-ZARI-PBL2^{UMP} complex using ZARI-RKS1 purified from insect cells and PBL2 purified from *Escherichia coli*. PBL2 coexpressed with AvrAC, but not when expressed alone, interacted with the RKS1-ZARI complex in gel filtration and pull-down assays (Fig. 3A and fig. S7). The lack

of AvrAC in the tertiary protein complex confirms that the AvrAC-mediated uridylylation of PBL2, but not AvrAC protein per se, is recognized by the ZARI-RKS1 receptor complex. We then solved a cryo-EM structure of the ZARI-RKS1-PBL2^{UMP} tertiary complex at a resolution of 4.3 Å (Fig. 3B and fig. S8). However, ZARI^{NBD} became much less well defined compared with that in the ZARI-RKS1 complex after PBL2^{UMP} binding, as indicated by the 3D reconstructions of the tertiary complex (Fig. 3C and fig. S8). Exclusion of this domain generated a 3D reconstruction with a resolution of 3.9 Å (Fig. 3B and fig. S8).

The model built into the higher resolution (3.9 Å) reconstruction of ZARI-RKS1-PBL2^{UMP} (table S1) is used for discussion of the RKS1-PBL2^{UMP} interaction. Consistent with the data from gel filtration (Fig. 3A), the structure of ZARI-RKS1-PBL2^{UMP} is monomeric (Fig. 4A). PBL2^{UMP} interacts exclusively with RKS1 (Fig. 4A), providing an explanation for AvrAC-induced recruitment of PBL2 to the ZARI-RKS1 complex (27). The loop region harboring the two uridylylated residues of PBL2^{UMP} is sandwiched between the N- and C-lobes of RKS1, mainly interacting with the activation segment of RKS1 (residues 213 to 243) (Fig. 4A). Additionally, the short α helix C-terminal to the uridylylated loop of PBL2 establishes contacts with the C-lobe of RKS1. The uridylyl moieties on PBL2^{Ser253, Thr254} form extensive polar and van der Waals interactions with residues 226 to 232 from the activation segment of RKS1 (Fig. 4B, top). On the opposite side, residues including Asp⁶⁹ and Val⁷⁰ make additional contacts with the uridylyl group of Ser²⁵³. These structural observations explain an essential role of uridylylation of these two residues in PBL2 interaction with RKS1 and the *avrAC*-specified disease resistance (27). The RKS1-PBL2^{UMP} interaction is further strengthened largely by hydrophobic packing of the C-lobe of RKS1 against the short α helix C-terminal to the uridylylated loop of PBL2 (Fig. 4B, bottom). Contrary to the ZARI-interacting residues of RKS1, the PBL2^{UMP}-interacting residues of RKS1 are not conserved among RLCK XII-2 subfamily proteins (fig. S4), explaining the specific recognition of RKS1 by PBL2.

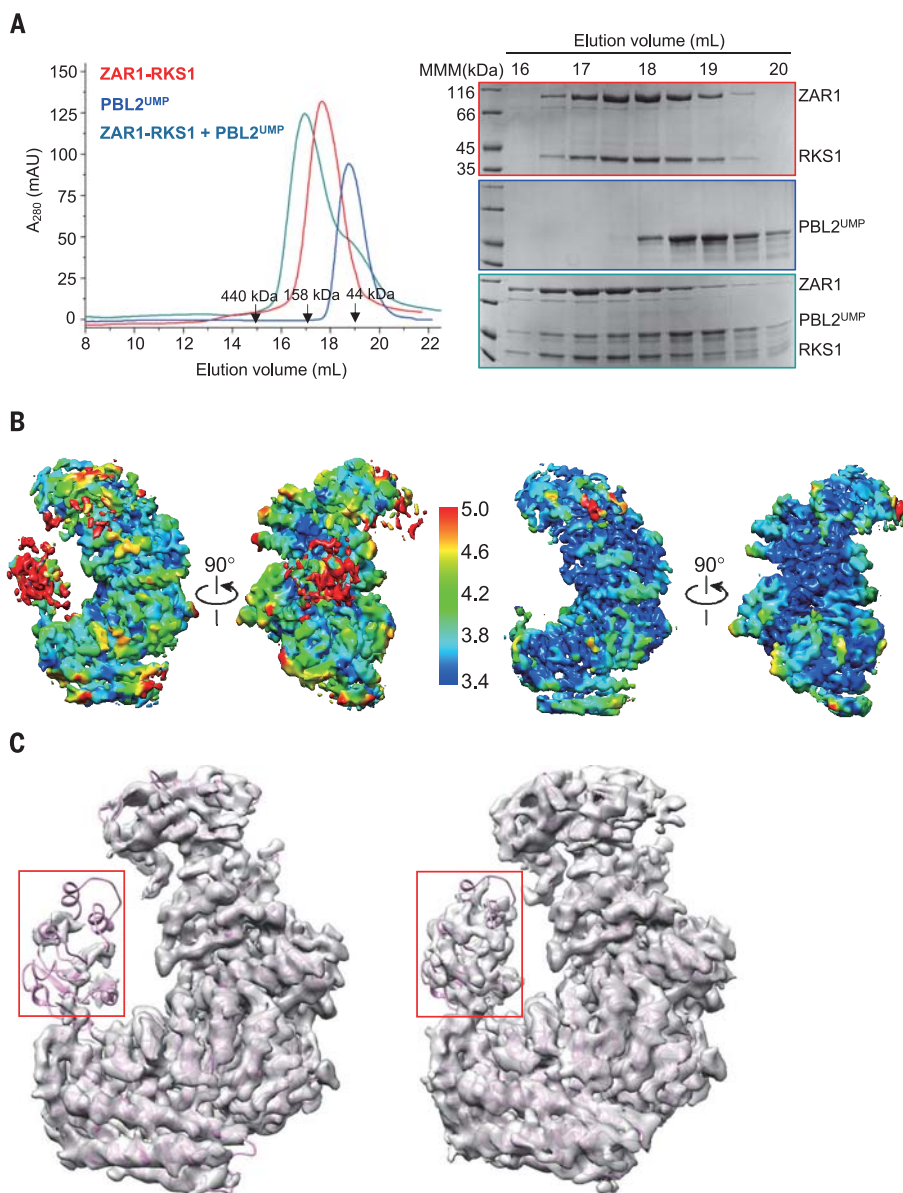
To further verify our structural observations, we made mutations in RKS1 and examined their effect on RKS1 interaction with PBL2^{UMP} using pull-down and co-IP assays. RKS1 itself was sufficient to interact with PBL2^{UMP} in the assays (fig. S9), as shown previously (27). By contrast, the PBL2^{UMP} binding activity was abolished or reduced by RKS1 mutations D69Y (Asp⁶⁹→Tyr), V70Y (Val⁷⁰→Tyr), G233A (Gly²³³→Ala), and T231Y (Thr²³¹→Tyr) (Fig. 4, C and D), a result predicted by the structural data (Fig. 4B, top). A similar result was also obtained for the RKS1 I235E (Ile²³⁵→Glu) mutant with a perturbed local conformation of the activation segment (Fig. 4, C and D). Gln⁶⁸ interacts intramolecularly with Lys⁷³ to stabilize the conformation of the loop carrying Asp⁶⁹ and Val⁷⁰. Consistently, the PBL2^{UMP}-binding activity of the RKS1 Q68Y

(Gln⁶⁸→Tyr) mutant was reduced compared with WT RKS1 (Fig. 4, C and D). Similarly, the RKS1 F232A (Phe²³²→Ala) and H240E (His²⁴⁰→Glu) mutations also decreased the interaction with PBL2^{UMP} in pull-down and co-IP assays (Fig. 4, C and D), supporting a role of Phe²³² and His²⁴⁰ in the interaction with the short α helix (Fig. 4B, bottom) of PBL2^{UMP}. We then tested the impact of these RKS1 mutations on AvrAC-induced cell death in protoplasts. When coexpressed with AvrAC, PBL2, and ZARI, the RKS1 mutants D69Y, T231Y, F232A, I235E, and H240E that are impaired in PBL2 interaction were abolished in cell death activity, whereas those with reduced PBL2^{UMP}-binding activity elicited weaker cell death compared with WT RKS1 (Fig. 4E). To further test these observations, we complemented the *rks1* mutant with *RKS1* variants by stable transformation and inoculated T1 transgenic plants with Xcc8004 or Δ *avrAC* strains. *rks1* mutant plants complemented with *RKS1*^{D69Y}, *RKS1*^{T231Y}, *RKS1*^{F232A}, and *RKS1*^{H240E} were fully susceptible to Xcc8004, indicating that these mutant variants were unable to confer *avrAC*-specified disease resistance in plants (Fig. 4F and fig. S10).

PBL2^{UMP} allosterically promotes the release of ADP from inactive ZARI

One revelation of the ZARI-RKS1-PBL2^{UMP} structure is that ZARI^{NBD} becomes more flexible after PBL2^{UMP} binding. Furthermore, structural comparison between ZARI-RKS1 and ZARI-RKS1-PBL2^{UMP} revealed that ZARI^{NBD} rotates about 60° outward. By contrast, the other domains of ZARI retain similar conformations to those observed in the inactive ZARI-RKS1 complex (Fig. 5A), providing an explanation for the monomeric, but still stable, ZARI-RKS1-PBL2^{UMP} complex. After PBL2^{UMP} binding, the conformation of RKS1 remains nearly unchanged except for its activation segment, which is flexible in the ZARI-RKS1 binary complex but becomes well defined in the ZARI-RKS1-PBL2^{UMP} tertiary complex (Fig. 5A and fig. S11). This result indicates that PBL2^{UMP} binding acts to stabilize the activation segment of RKS1. Structural comparison further showed that the PBL2^{UMP}-stabilized segment of RKS1 collides with one end of the ADP-bound ZARI^{NBD} from the inactive RKS1-ZARI complex (Fig. 5A). The steric clash is expected to dislocate ZARI^{NBD} of the inactive ZARI, resulting in conformational changes in it, as observed in the structure. The conformational incompatibility between the PBL2^{UMP}-bound RKS1 and the ADP-bound ZARI^{NBD} suggests that the PBL2^{UMP} recruitment can indirectly impede the ADP-binding activity of ZARI, thus releasing ADP from its inactive form. To further support this hypothesis, we tested the ADP-binding activity of the RKS1-ZARI complex in the presence of PBL2^{UMP} or PBL2 using the assay previously described (40). Indeed, PBL2^{UMP} induced ADP release from the ZARI-RKS1 complex with much higher efficiency than PBL2 (Fig. 5B). Taken together, our structural and biochemical data indicate that PBL2^{UMP} binding functions to stabilize

Fig. 3. PBL2^{UMP} interaction with ZAR1-RKS1 enhances ZAR1^{NBD} flexibility. (A) ZAR1-RKS1 and PBL2^{UMP} form a monomeric tertiary complex in gel filtration. Shown on the left are gel filtration profiles of ZAR1-RKS1 (red), PBL2^{UMP} (blue), and ZAR1-RKS1+PBL2^{UMP} (cyan) proteins. Positions of standard molecular mass are indicated by arrows. A₂₈₀, absorbance at 280 nm; mAU, milli-absorbance units. Peak fractions in the left were visualized by SDS-PAGE followed by Coomassie blue staining and are shown on the right. MMM, molecular mass marker. (B) 3D reconstructions of the ZAR1-RKS1-PBL2^{UMP} complex. Two orientations of the final EM density maps of the ZAR1-RKS1-PBL2^{UMP} complex with ZAR1^{NBD} unmasked (the two on the left) and masked (the two on the right). Shown in the middle is the color scale, in angstroms, for local resolution of the density maps. (C) ZAR1^{NBD} is much less well defined than the remaining parts of the ZAR1-RKS1-PBL2^{UMP} complex. Shown on the left and right are EM densities of the ZAR1-RKS1-PBL2^{UMP} complex contoured at 4.0 σ and 2.0 σ , respectively. ZAR1^{NBD} is highlighted in the red frames.



the activation segment of RKS1, which sterically hinders ADP binding of ZAR1. This mechanism may also be true with HopZ1a-induced activation of ZAR1. However, in contrast with RKS1, ZEDI was reported to interact with ZAR1^{CC} in addition to ZAR1^{LRR} (29), suggesting that RKS1 and ZEDI might have different roles in ZAR1 activation.

Discussion

Autoinhibition, ligand recognition, and nucleotide exchange mechanisms of ZAR1

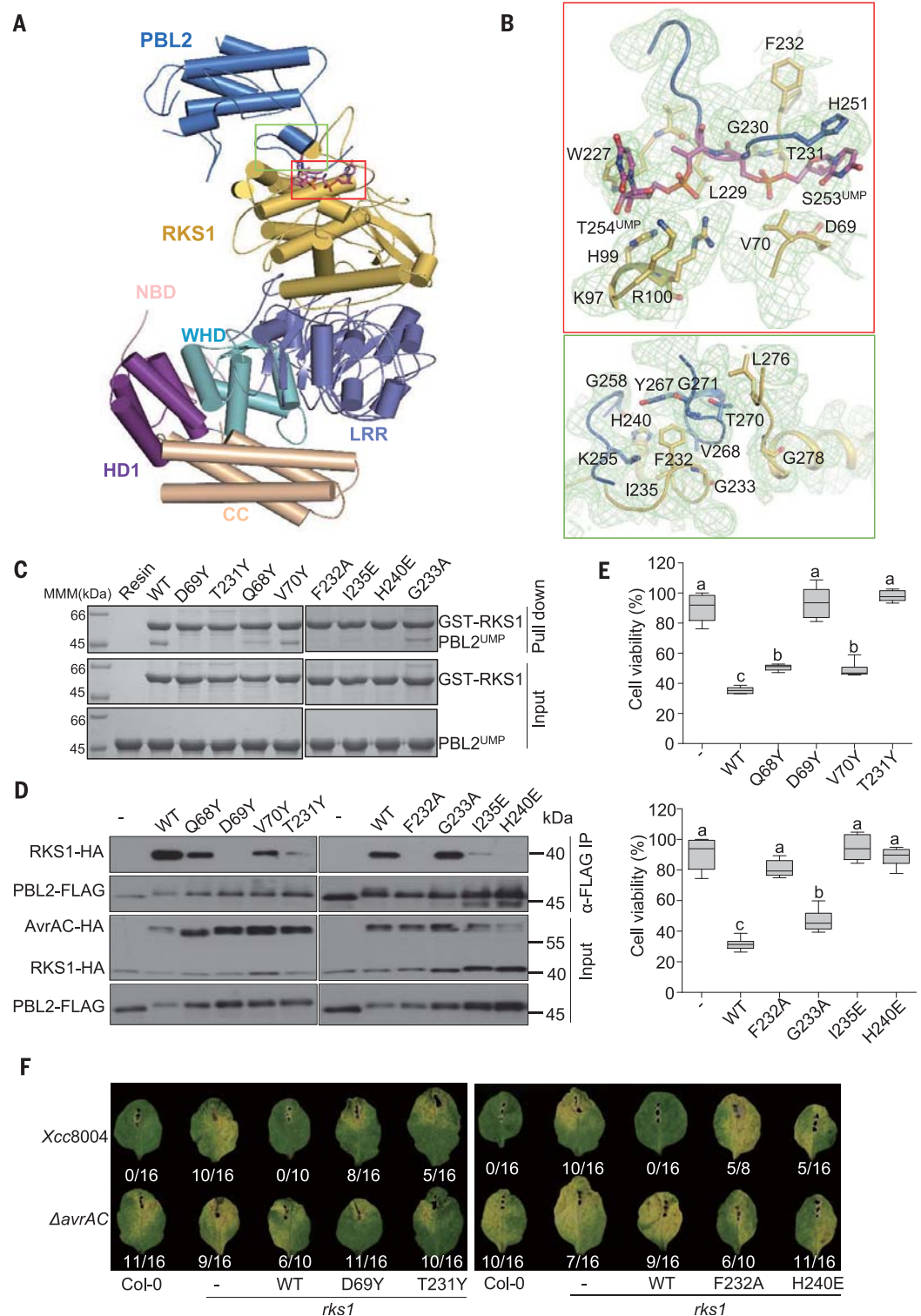
Our structural and biochemical understanding of plant NLRs largely comes from studies of animal NLRs, Apaf-1, and CED-4 (41). However, despite their analogous domains, NLRs from animals and plants resulted from convergent evolution after independent origins (42). Furthermore, although nucleotide exchange (ADP with ATP) is widely believed to have roles

in NLR-initiated signaling (3), the underlying mechanism remained elusive, particularly because the bound ADP molecule is deeply buried, as demonstrated in the inactive NLRC4 (12) and Apaf-1 (9, 11). In this study, we report the cryo-EM structures of the plant NLR protein ZAR1 not only in its inactive ADP-bound state but also an intermediate state that is likely nucleotide-free in vitro because of the dislodged NBD. The structures revealed that ZAR1 assumes a canonical NOD structure as observed in NLRC4 (12) and Apaf-1 (9, 11) and that ADP binding functions to maintain its inactive conformation (Fig. 1). Despite the conserved NOD structure shared by these proteins, the C-terminal ZAR1^{LRR} is presented in a position different from its counterpart of NLRC4 or Apaf-1. Nonetheless, the specially positioned ZAR1^{LRR} still acts to sequester ZAR1 in a monomeric and ADP-bound state, which is further

stabilized by ZAR1^{CC} via interaction with ZAR1^{LRR}, ZAR1^{WHD}, and ZAR1^{HDD1}. ZAR1^{LRR} is primarily responsible for ZAR1 interaction with RKS1 (Fig. 2A), whereas recognition of PBL2^{UMP} occurs exclusively through RKS1 from the preformed ZAR1-RKS1 complex (Fig. 4A). The data provide the first structural view of recognition of modified self by NLRs in animals (43, 44) and plants (3, 4, 7, 8). Furthermore, capturing the likely nucleotide-free ZAR1 structure provides insights into the nucleotide exchange mechanism of the NLR. Structural comparison showed that the stabilized activation segment of RKS1 induced by PBL2^{UMP} sterically clashes with the ADP-bound ZAR1^{NBD} (Fig. 5A), which is expected to induce a substantial distortion of the structural domain, resulting in its dislodgement from the inactive conformation and consequently an ADP-depleted ZAR1. Such structural plasticity of the ATPase domain was also observed in the AAA+

Fig. 4. RKS1-mediated PBL2^{UMP} recognition by the ZARI-RKS1.

(A) Overall structure of the ZARI-RKS1-PBL2^{UMP} complex. The red and green frames highlight the interacting regions between RKS1 and PBL2^{UMP}. (B) Detailed interactions of uridylated PBL2^{UMP} with RKS1 (top) and an α helix of PBL2^{UMP} with RKS1 (bottom), corresponding to the red- and green-framed regions in (A). Cryo-EM density is shown in green mesh. (C) Mutations of RKS1 around the two interfaces shown in (B) affect RKS1 interaction with PBL2^{UMP} in vitro. GST-tagged RKS1 bound to GS4B beads was incubated with an excess amount of PBL2^{UMP}. After extensive washing, the beads were analyzed by SDS-PAGE and Coomassie brilliant blue staining. (D) Mutations of RKS1 around the two interfaces shown in (B) diminish RKS1 interaction with PBL2^{UMP} in protoplasts. Protoplasts isolated from *rks1* plants were transfected with the indicated constructs for co-IP assays as in Fig. 2F. (E) Mutations of RKS1 around the two interfaces shown in (B) reduce AvrAC-induced cell death in protoplasts. The assays were performed as in Fig. 2G. Different letters indicate significant difference ($P < 0.05$, Tukey post hoc test). (F) Mutations of RKS1 around the two interfaces shown in (B) impair *avrAC*-specified resistance in *Arabidopsis* plants. *rks1* mutant plants were complemented with the indicated variants of RKS1. Transgenic plants of the T1 generation were inoculated with the indicated bacterial strains and scored for disease symptoms as in Fig. 2H.



protein p97, with its NBD undergoing order-disorder transitions during the hydrolysis cycle (45). The mechanism of PBL2^{UMP}-induced ADP release from inactive ZARI resembles that of HspBP1-catalyzed nucleotide exchange of eukaryotic Hsp70 (46). Collectively, our results offer structural insights into the autoinhibition, ligand recognition, and nucleotide exchange

mechanisms of ZARI, providing a template for understanding of other NLRs from plants and animals.

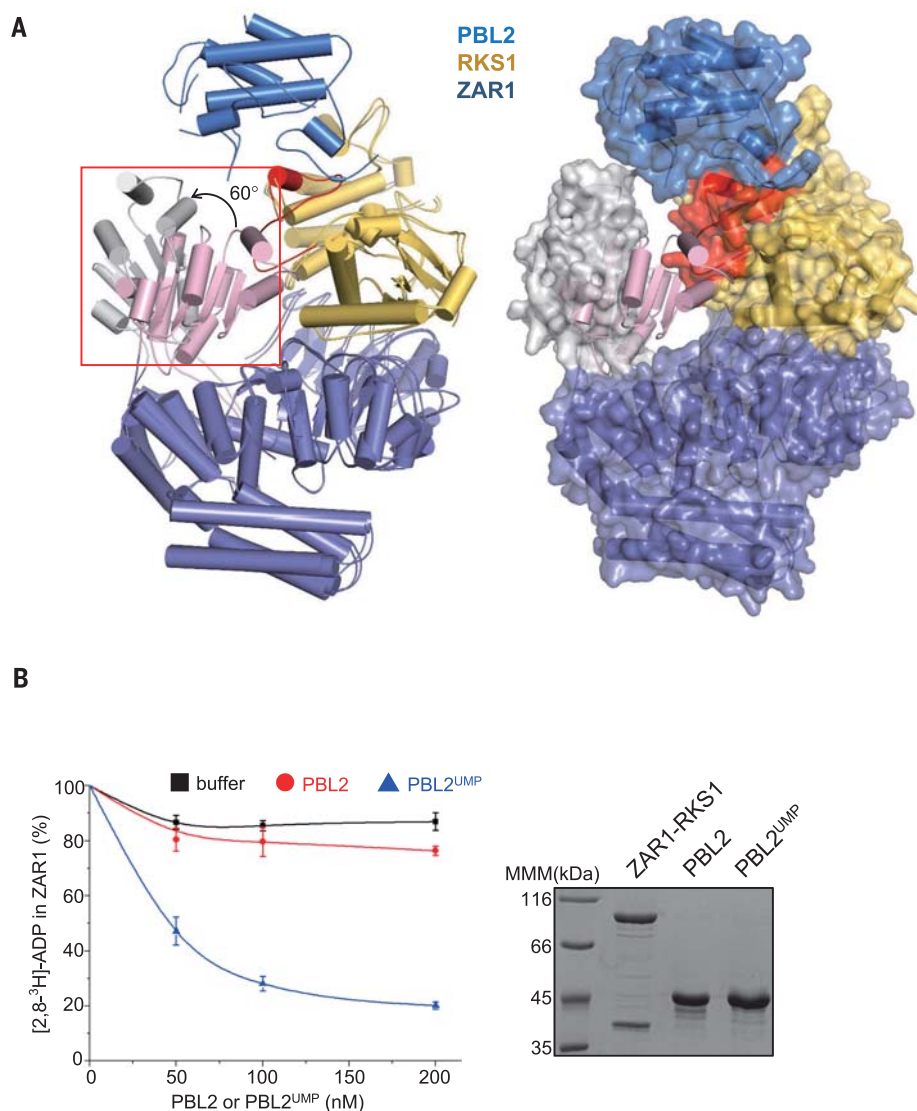
RKS1 functions as a nucleotide exchange factor

Indirect recognition of effectors by plant NLRs can occur through effector-mediated post-

translational modifications of plant sensor proteins, such as the recognition of AvrAC by ZARI (27). Thus, PBL2^{UMP} acts as a ligand for the ZARI-RKS1 complex. Our structural and biochemical data showed that PBL2^{UMP} indirectly triggers the release of ADP from the inactive ZARI (Fig. 5). However, structural comparison revealed that ADP release is not accompanied

Fig. 5. PBL2^{UMP} binding allosterically promotes ADP release from ZAR1.

(A) PBL2^{UMP} binding stabilizes a segment of RKS1 that is conformationally incompatible with ZAR1^{NBD} in ZAR1-RKS1. Shown on the left and right are structural superpositions of ZAR1-RKS1 and ZAR1-RKS1-PBL2^{UMP}. ZAR1-RKS1-PBL2^{UMP} on the right is shown in both cartoon and transparent surface. ZAR1^{NBD} domains from ZAR1-RKS1 and ZAR1-RKS1-PBL2^{UMP} are shown in gray and pink, respectively. The activation segment of RKS1 (colored in red) is flexible in ZAR1-RKS1, but well defined in ZAR1-RKS1-PBL2^{UMP}. The red frame on the left highlights ZAR1^{NBD}. **(B)** Recruitment of PBL2^{UMP} greatly reduces ADP-binding activity of the ZAR1-RKS1 complex. An aliquot of [2,8-³H]-ADP-bound ZAR1-RKS1 (6×His fused to the C terminus of ZAR1) was incubated with different concentrations of PBL2 or PBL2^{UMP} at 4°C for 30 min. After flowing the samples through Ni-resins, the [2,8-³H]-ADP bound by ZAR1 was quantified by scintillation counting (left). The data were normalized against the input and are presented as percentages. Data are represented as mean ± SEM (*n* = 3). The proteins used for the ADP release assay are shown on the right.



with conformational changes in the C-terminal ZAR1^{LRR} domain, as proposed for activation of plant NLR proteins (47, 48). Furthermore, PBL2^{UMP} induced no oligomerization of ZAR1 in vitro, similar to what has been observed with cytochrome c binding to Apaf-1 in the absence of ATP or dATP (10), though whether the cytochrome c-bound Apaf-1 is nucleotide-free or not remains undetermined. These results collectively indicate that the primary function of PBL2^{UMP} is to prime the release of ADP from the inactive form of ZAR1 for activation. This sharply contrasts with flagellin binding to the NLR NAIP5 in animals (49, 50), in which flagellin functions to stabilize the active conformation of the NLR protein. The PBL2^{UMP}-primed ADP release from the inactive ZAR1 is directly mediated by RKS1. This biochemical function of RKS1 is reminiscent of the nucleotide exchange factors (NEFs) of Hsp70 (51), which have critical roles in the functional cycle of Hsp70s by facilitating the release of ADP from its inactive state. Thus, RKS1 in the preformed ZAR1-RKS1 complex

can be understood as an inactive NEF, whose activity is induced by PBL2^{UMP}. NEFs of Hsp70s, despite their conserved biochemical function, are structurally unrelated and mechanistically highly diverse in nucleotide exchange reactions (51). Because nucleotide exchange is likely a general mechanism for plant NLR activation, as further confirmed in the accompanying study (52), it is conceivable that some other effector proteins indirectly recognized by plant NLRs similarly trigger NLR activation via inducing potential NEF activities of NLR-guarded host proteins. The study presented here provides a template for the analyses of other plant NLRs.

Model for ZAR1 priming

The data presented here and previously (10, 13, 14, 31, 32) support a stepwise activation model of ZAR1 (Fig. 6). ADP binding and the intramolecular interactions among multiple domains act collectively to keep ZAR1 in an inactive state. The C-terminal ZAR1^{LRR} domain mediates formation of the preformed ZAR1-

RKS1 complex that recognizes the AvrAC-uridylylated PBL2. Binding of PBL2^{UMP} to the preformed ZAR1-RKS1 complex activates the NEF activity of RKS1, thus releasing ADP from ZAR1. ADP release, however, does not result in full activation of ZAR1, because ZAR1 is still monomeric and adopts a similar conformation to the ADP-bound ZAR1 except its NBD. This indicates that the ADP-depleted form of ZAR1 is in an intermediate state. The primed, but not oligomerized, ZAR1-RKS1-PBL2^{UMP} suggests that a second step involving structural reorganizations similar to those for NLRC4 and Apaf-1 activation is required to fully activate ZAR1. ATP or dATP is the best candidate molecule for binding to the ADP-free ZAR1 to trigger the second signaling step, as observed for activation of Apaf-1. ZAR1 activation after ATP or dATP binding likely involves oligomerization of the NLR protein, a hallmark of AAA+ family proteins (53). In this model, a fail-safe mechanism is used by ZAR1 for its activation, wherein the AvrAC-modified PBL2 acts as a key to unlock ZAR1, but the

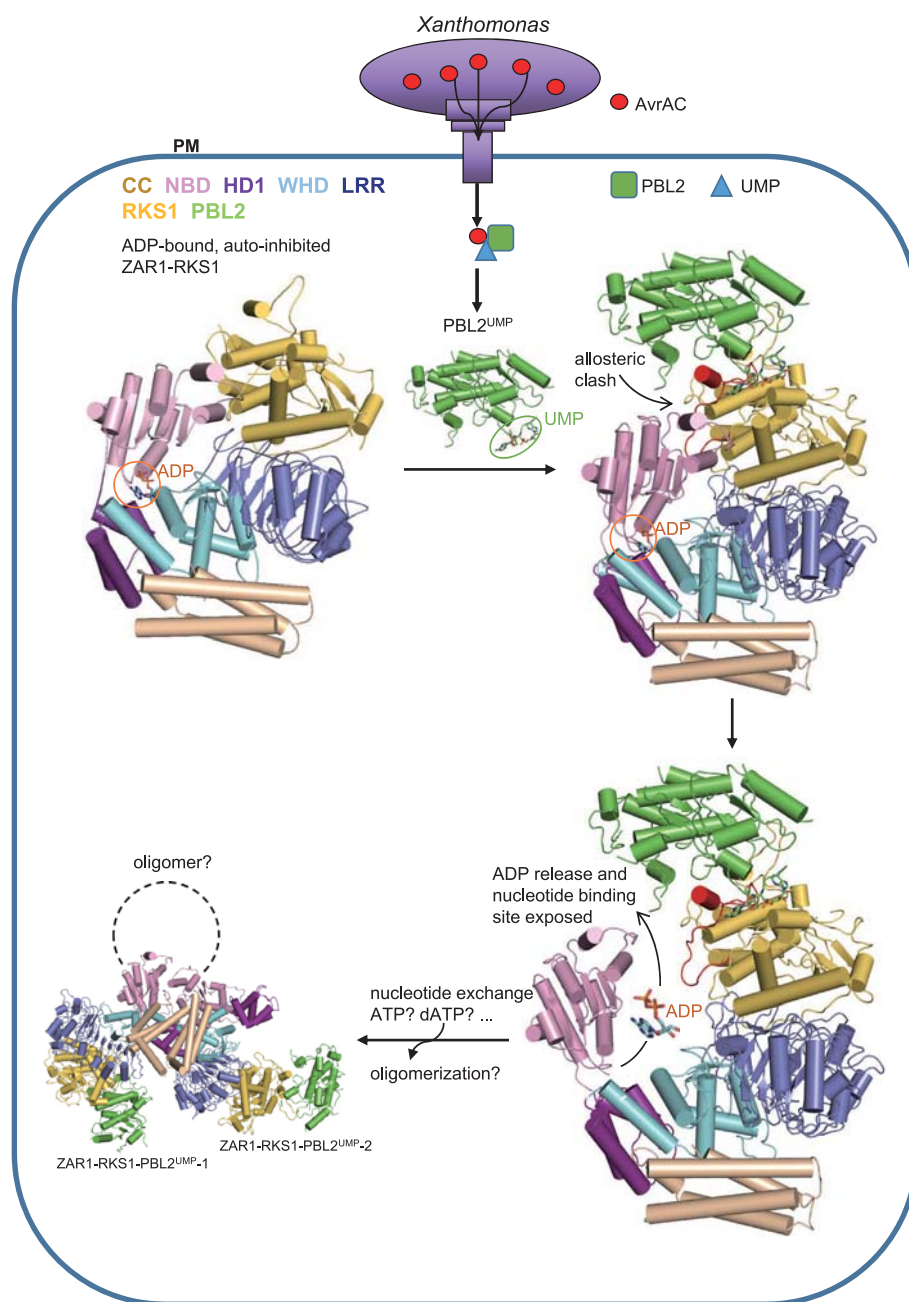


Fig. 6. Model for the PBL2^{UMP}-induced priming of the ZAR1 complex. ADP binding and intramolecular interaction of various ZAR1 domains in the preformed ZAR1-RKS1 complex maintains ZAR1 in an inactive conformation. The *X. campestris* pv. *campestris* effector AvrAC uridylylates PBL2, allowing the latter to be recruited by ZAR1-RKS1. The binding of PBL2^{UMP} to RKS1 stabilizes the activation segment of RKS1, which causes a steric hindrance with ZAR1^{NBD}. The dislodged ZAR1^{NBD} releases ADP, and the ZAR1-RKS1-PBL2^{UMP} enters into an intermediate state, which is likely competent for ATP binding and full activation of ZAR1.

unlocked ZAR1 is not fully activated until it binds to a second signaling molecule.

Materials and methods summary

ZAR1 and RKS1 (with an N-terminal 6×His-SUMO) were coexpressed in Sf21 insect cells. The complex protein was first purified using Ni-NTA and further cleaned by ion-exchange and gel filtration after removal of SUMO by

PreScission. The purified ZAR1-RKS1 was concentrated to ~1.0 mg/ml for cryo-EM. Similar protocols were used to purify the RKS1 mutants in complex with ZAR1. To purify ZAR1 mutants complexed with RKS1, N-terminally GST-tagged ZAR1 and RKS1 were coexpressed in Sf21 insect cells and the mutant complex proteins were purified by Glutathione Sepharose 4B. AvrAC and PBL2 (with a C-terminal 6×His tag) were

coexpressed in *E. coli*. The PBL2^{UMP} protein was purified using the protocols described above. The purified ZAR1-RKS1 and PBL2^{UMP} proteins were mixed together and then subjected to gel filtration to purify the ZAR1-RKS1-PBL2^{UMP} complex. The complex was concentrated to ~1.5 mg/ml for cryo-EM. To assay ZAR1-RKS1 interaction with PBL2^{UMP} or PBL2, the purified ZAR1-RKS1 was incubated with the His-tagged PBL2^{UMP} or PBL2 and bound to Ni resins. After washing, the Ni beads were analyzed by SDS-PAGE and Coomassie brilliant blue staining.

To assay the effect of PBL2 or PBL2^{UMP} on the ADP-binding activity of ZAR-RKS1, the [2,8-³H]-ADP-ZAR1-RKS1 complex protein bound to Ni resins was incubated with different concentrations of PBL2 or PBL2^{UMP}, and then each sample was pelleted by centrifugation. After washing, the pellet was eluted with 250 mM imidazole, and [2,8-³H]-ADP in the eluent was quantified by scintillation counting.

Cryo-EM data of frozen hydrated grids of ZAR1-RKS1 or ZAR1-RKS1-PBL2^{UMP} were collected on a Titan Krios electron microscope operated at 300 kV equipped with VPP (Volta Phase Plate) and a Gatan K2 Summit direct electron detection camera (Gatan) using AutoEMation. The ZAR1-RKS1-PBL2^{UMP} dataset was collected without the insertion of VPP, and the ZAR1-RKS1 dataset was collected using VPP, as described earlier. The raw supersolution dose-fractionated image stacks were binned, aligned, dose-weighted, and summed using MotionCor2. Contrast transfer function (CTF) parameters were estimated using CTFFIND4 and GCTF. Particle picking, 2D classification, 3D classification, and refinement were all performed in RELION. The EM density reconstructed from ZAR1-RKS1 was used for model building in Chimera (54) and COOT. To build the model of ZAR1-RKS1-PBL2^{UMP}, the refined model of ZAR1-RKS1 without ZAR1^{NBD} was fitted into the EM density reconstructed from the former complex in Chimera. The crystal structure of the BAK1 kinase domain was used as the initial model of PBL2^{UMP}. The final models were refined against their corresponding EM maps by PHENIX.

Structure-guided mutagenesis was carried out to assess the importance of various amino acid residues in ZAR1-RKS1 and RKS1-PBL2^{UMP} interactions, cell-death triggering, and resistance in plants. Wild-type and mutant forms of ZAR1, RKS1, PBL2, and AvrAC constructs were transfected into *Arabidopsis* protoplasts, and cell viability was determined. RKS1 or ZAR1 variants under the control of native promoters were introduced into *rks1* or *zar1* mutants, respectively, and stable transgenic plants were wound-inoculated with *Xanthomonas campestris* pv. *campestris* strains carrying or lacking *avrAC*. Disease resistance was scored on the basis of presence or absence of disease symptoms.

REFERENCES AND NOTES

1. M. Antolin-Llovera, M. K. Ried, A. Binder, M. Parniske, Receptor kinase signaling pathways in plant-microbe interactions. *Annu. Rev. Phytopathol.* **50**, 451–473 (2012). doi: 10.1146/annurev-phyto-081211-173002; pmid: 22920561

2. D. Tang, G. Wang, J. M. Zhou, Receptor kinases in plant-pathogen interactions: More than pattern recognition. *Plant Cell* **29**, 618–637 (2017). doi: [10.1105/tpc.16.00891](https://doi.org/10.1105/tpc.16.00891); pmid: [28302675](https://pubmed.ncbi.nlm.nih.gov/28302675/)
3. J. D. Jones, R. E. Vance, J. L. Dangl, Intracellular innate immune surveillance devices in plants and animals. *Science* **354**, aaf6395 (2016). doi: [10.1126/science.aaf6395](https://doi.org/10.1126/science.aaf6395); pmid: [27934708](https://pubmed.ncbi.nlm.nih.gov/27934708/)
4. X. Zhang, P. N. Dodds, M. Bernoux, What do we know about NOD-like receptors in plant immunity? *Annu. Rev. Phytopathol.* **55**, 205–229 (2017). doi: [10.1146/annurev-phyto-080516-035250](https://doi.org/10.1146/annurev-phyto-080516-035250); pmid: [28637398](https://pubmed.ncbi.nlm.nih.gov/28637398/)
5. T. Maekawa, T. A. Kufer, P. Schulze-Lefert, NLR functions in plant and animal immune systems: So far and yet so close. *Nat. Immunol.* **12**, 817–826 (2011). doi: [10.1038/ni.2083](https://doi.org/10.1038/ni.2083); pmid: [21852785](https://pubmed.ncbi.nlm.nih.gov/21852785/)
6. D. D. Leipe, E. V. Koonin, L. Aravind, STAND, a class of P-loop NTPases including animal and plant regulators of programmed cell death: Multiple, complex domain architectures, unusual phyletic patterns, and evolution by horizontal gene transfer. *J. Mol. Biol.* **343**, 1–28 (2004). doi: [10.1016/j.jmb.2004.08.023](https://doi.org/10.1016/j.jmb.2004.08.023); pmid: [15381417](https://pubmed.ncbi.nlm.nih.gov/15381417/)
7. J. L. Dangl, D. M. Horvath, B. J. Staskawicz, Pivoting the plant immune system from dissection to deployment. *Science* **341**, 746–751 (2013). doi: [10.1126/science.1236011](https://doi.org/10.1126/science.1236011); pmid: [23950531](https://pubmed.ncbi.nlm.nih.gov/23950531/)
8. J. Kourelis, R. A. L. van der Hoorn, Defended to the nines: 25 years of resistance gene cloning identifies nine mechanisms for R protein function. *Plant Cell* **30**, 285–299 (2018). doi: [10.1105/tpc.17.00579](https://doi.org/10.1105/tpc.17.00579); pmid: [29382771](https://pubmed.ncbi.nlm.nih.gov/29382771/)
9. T. F. Reubold, S. Wohlgemuth, S. Eschenburg, Crystal structure of full-length Apaf-1: How the death signal is relayed in the mitochondrial pathway of apoptosis. *Structure* **19**, 1074–1083 (2011). doi: [10.1016/j.str.2011.05.013](https://doi.org/10.1016/j.str.2011.05.013); pmid: [21827944](https://pubmed.ncbi.nlm.nih.gov/21827944/)
10. M. Zhou et al., Atomic structure of the apoptosome: Mechanism of cytochrome c- and dATP-mediated activation of Apaf-1. *Genes Dev.* **29**, 2349–2361 (2015). doi: [10.1101/gad.272278.115](https://doi.org/10.1101/gad.272278.115); pmid: [26543158](https://pubmed.ncbi.nlm.nih.gov/26543158/)
11. S. J. Riedl, W. Li, Y. Chao, R. Schwarzenbacher, Y. Shi, Structure of the apoptotic protease-activating factor 1 bound to ADP. *Nature* **434**, 926–933 (2005). doi: [10.1038/nature03465](https://doi.org/10.1038/nature03465); pmid: [15829969](https://pubmed.ncbi.nlm.nih.gov/15829969/)
12. Z. Hu et al., Crystal structure of NLRC4 reveals its autoinhibition mechanism. *Science* **341**, 172–175 (2013). doi: [10.1126/science.1236381](https://doi.org/10.1126/science.1236381); pmid: [23765277](https://pubmed.ncbi.nlm.nih.gov/23765277/)
13. Z. Hu et al., Structural and biochemical basis for induced self-propagation of NLRC4. *Science* **350**, 399–404 (2015). doi: [10.1126/science.aac5489](https://doi.org/10.1126/science.aac5489); pmid: [26449475](https://pubmed.ncbi.nlm.nih.gov/26449475/)
14. L. Zhang et al., Cryo-EM structure of the activated NAIP2-NLRC4 inflammasome reveals nucleated polymerization. *Science* **350**, 404–409 (2015). doi: [10.1126/science.aac5789](https://doi.org/10.1126/science.aac5789); pmid: [26449474](https://pubmed.ncbi.nlm.nih.gov/26449474/)
15. S. Maekawa, U. Ohto, T. Shibata, K. Miyake, T. Shimizu, Crystal structure of NOD2 and its implications in human disease. *Nat. Commun.* **7**, 11813 (2016). doi: [10.1038/ncomms11813](https://doi.org/10.1038/ncomms11813); pmid: [27283905](https://pubmed.ncbi.nlm.nih.gov/27283905/)
16. W. I. Tameling et al., The tomato R gene products I-2 and MI-1 are functional ATP binding proteins with ATPase activity. *Plant Cell* **14**, 2929–2939 (2002). doi: [10.1105/tpc.005793](https://doi.org/10.1105/tpc.005793); pmid: [12417711](https://pubmed.ncbi.nlm.nih.gov/12417711/)
17. S. J. Williams et al., An autoactive mutant of the M flax rust resistance protein has a preference for binding ATP, whereas wild-type M protein binds ADP. *Mol. Plant Microbe Interact.* **24**, 897–906 (2011). doi: [10.1094/MPMI-03-11-0052](https://doi.org/10.1094/MPMI-03-11-0052); pmid: [21539434](https://pubmed.ncbi.nlm.nih.gov/21539434/)
18. M. Bernoux et al., Comparative analysis of the flax immune receptors L6 and L7 suggests an equilibrium-based switch activation model. *Plant Cell* **28**, 146–159 (2016). doi: [10.1105/tpc.16.00428](https://doi.org/10.1105/tpc.16.00428); pmid: [26744216](https://pubmed.ncbi.nlm.nih.gov/26744216/)
19. G. J. Rairdan et al., The coiled-coil and nucleotide binding domains of the potato Rx disease resistance protein function in pathogen recognition and signaling. *Plant Cell* **20**, 739–751 (2008). doi: [10.1105/tpc.107.056036](https://doi.org/10.1105/tpc.107.056036); pmid: [18344282](https://pubmed.ncbi.nlm.nih.gov/18344282/)
20. J. G. Ellis, G. J. Lawrence, J. E. Luck, P. N. Dodds, Identification of regions in alleles of the flax rust resistance gene L that determine differences in gene-for-gene specificity. *Plant Cell* **11**, 495–506 (1999). doi: [10.1105/tpc.11.3.495](https://doi.org/10.1105/tpc.11.3.495); pmid: [10072407](https://pubmed.ncbi.nlm.nih.gov/10072407/)
21. Y. Jia, S. A. McAdams, G. T. Bryan, H. P. Hershey, B. Valent, Direct interaction of resistance gene and avirulence gene products confers rice blast resistance. *EMBO J.* **19**, 4004–4014 (2000). doi: [10.1093/emboj/19.15.4004](https://doi.org/10.1093/emboj/19.15.4004); pmid: [10921881](https://pubmed.ncbi.nlm.nih.gov/10921881/)
22. P. N. Dodds, G. J. Lawrence, J. G. Ellis, Six amino acid changes confined to the leucine-rich repeat β -strand/ β -turn motif determine the difference between the P and P2 rust resistance specificities in flax. *Plant Cell* **13**, 163–178 (2001). doi: [10.1105/tpc.13.01.163](https://doi.org/10.1105/tpc.13.01.163); pmid: [11158537](https://pubmed.ncbi.nlm.nih.gov/11158537/)
23. L. Deslandes et al., Physical interaction between RRS1-R, a protein conferring resistance to bacterial wilt, and PopP2, a type III effector targeted to the plant nucleus. *Proc. Natl. Acad. Sci. U.S.A.* **100**, 8024–8029 (2003). doi: [10.1073/pnas.1230660100](https://doi.org/10.1073/pnas.1230660100); pmid: [12788974](https://pubmed.ncbi.nlm.nih.gov/12788974/)
24. Q. H. Shen et al., Recognition specificity and RARI/SGTI dependence in barley Mla disease resistance genes to the powdery mildew fungus. *Plant Cell* **15**, 732–744 (2003). doi: [10.1105/tpc.009258](https://doi.org/10.1105/tpc.009258); pmid: [12615945](https://pubmed.ncbi.nlm.nih.gov/12615945/)
25. C. I. Wang et al., Crystal structures of flax rust avirulence proteins AvrL567-A and -D reveal details of the structural basis for flax disease resistance specificity. *Plant Cell* **19**, 2898–2912 (2007). doi: [10.1105/tpc.107.053611](https://doi.org/10.1105/tpc.107.053611); pmid: [17873095](https://pubmed.ncbi.nlm.nih.gov/17873095/)
26. J. D. Lewis et al., The Arabidopsis ZED1 pseudokinase is required for ZARI-mediated immunity induced by the *Pseudomonas syringae* type III effector HopZ1a. *Proc. Natl. Acad. Sci. U.S.A.* **110**, 18722–18727 (2013). doi: [10.1073/pnas.1315520110](https://doi.org/10.1073/pnas.1315520110); pmid: [24170858](https://pubmed.ncbi.nlm.nih.gov/24170858/)
27. G. Wang et al., The decoy substrate of a pathogen effector and a pseudokinase specify pathogen-induced modified-self recognition and immunity in plants. *Cell Host Microbe* **18**, 285–295 (2015). doi: [10.1016/j.chom.2015.08.004](https://doi.org/10.1016/j.chom.2015.08.004); pmid: [26355215](https://pubmed.ncbi.nlm.nih.gov/26355215/)
28. D. Seto et al., Expanded type III effector recognition by the ZARI NLR protein using ZED1-related kinases. *Nat. Plants* **3**, 17027 (2017). doi: [10.1038/nplants.2017.27](https://doi.org/10.1038/nplants.2017.27); pmid: [28288096](https://pubmed.ncbi.nlm.nih.gov/28288096/)
29. M. Baudin, J. A. Hassan, K. J. Schreiber, J. D. Lewis, Analysis of the ZARI immune complex reveals determinants for immunity and molecular interactions. *Plant Physiol.* **174**, 2038–2053 (2017). doi: [10.1104/pp.17.00441](https://doi.org/10.1104/pp.17.00441); pmid: [28652264](https://pubmed.ncbi.nlm.nih.gov/28652264/)
30. A. Schultink, T. Qi, J. Bally, B. Staskawicz, Using forward genetics in *Nicotiana benthamiana* to uncover the immune signaling pathway mediating recognition of the *Xanthomonas perforans* effector XopJ4. *New Phytol.* **221**, 1001–1009 (2019). doi: [10.1111/nph.15411](https://doi.org/10.1111/nph.15411); pmid: [30156705](https://pubmed.ncbi.nlm.nih.gov/30156705/)
31. S. Qi et al., Crystal structure of the *Caenorhabditis elegans* apoptosome reveals an octameric assembly of CED-4. *Cell* **141**, 446–457 (2010). doi: [10.1016/j.cell.2010.03.017](https://doi.org/10.1016/j.cell.2010.03.017); pmid: [20434985](https://pubmed.ncbi.nlm.nih.gov/20434985/)
32. Y. Pang et al., Structure of the apoptosome: Mechanistic insights into activation of an initiator caspase from *Drosophila*. *Genes Dev.* **29**, 277–287 (2015). doi: [10.1101/gad.255877.114](https://doi.org/10.1101/gad.255877.114); pmid: [25644603](https://pubmed.ncbi.nlm.nih.gov/25644603/)
33. L. Franchi, R. Muñoz-Planillo, G. Núñez, Sensing and reacting to microbes through the inflammasomes. *Nat. Immunol.* **13**, 325–332 (2012). doi: [10.1038/ni.2231](https://doi.org/10.1038/ni.2231); pmid: [22430785](https://pubmed.ncbi.nlm.nih.gov/22430785/)
34. V. A. Rathinam, S. K. Vanaja, K. A. Fitzgerald, Regulation of inflammasome signaling. *Nat. Immunol.* **13**, 333–342 (2012). doi: [10.1038/ni.2237](https://doi.org/10.1038/ni.2237); pmid: [22430786](https://pubmed.ncbi.nlm.nih.gov/22430786/)
35. E. A. Van Der Biezen, J. D. Jones, Plant disease-resistance proteins and the gene-for-gene concept. *Trends Biochem. Sci.* **23**, 454–456 (1998). doi: [10.1016/S0968-0004\(98\)01311-5](https://doi.org/10.1016/S0968-0004(98)01311-5); pmid: [9868361](https://pubmed.ncbi.nlm.nih.gov/9868361/)
36. W. I. Tameling et al., Mutations in the NB-ARC domain of I-2 that impair ATP hydrolysis cause autoactivation. *Plant Physiol.* **140**, 1233–1245 (2006). doi: [10.1104/pp.105.073510](https://doi.org/10.1104/pp.105.073510); pmid: [16489136](https://pubmed.ncbi.nlm.nih.gov/16489136/)
37. W. Hao, S. M. Collier, P. Moffett, J. Chai, Structural basis for the interaction between the potato virus X resistance protein (Rx) and its cofactor Ran GTPase-activating protein 2 (RanGAP2). *J. Biol. Chem.* **288**, 35868–35876 (2013). doi: [10.1074/jbc.M113.517417](https://doi.org/10.1074/jbc.M113.517417); pmid: [24194517](https://pubmed.ncbi.nlm.nih.gov/24194517/)
38. L. W. Casey et al., The CC domain structure from the wheat stem rust resistance protein Sr33 challenges paradigms for dimerization in plant NLR proteins. *Proc. Natl. Acad. Sci. U.S.A.* **113**, 12856–12861 (2016). doi: [10.1073/pnas.1609922113](https://doi.org/10.1073/pnas.1609922113); pmid: [27791121](https://pubmed.ncbi.nlm.nih.gov/27791121/)
39. F. El Kasmi et al., Signaling from the plasma-membrane localized plant immune receptor RPM1 requires self-association of the full-length protein. *Proc. Natl. Acad. Sci. U.S.A.* **114**, E7385–E7394 (2017). doi: [10.1073/pnas.1708288114](https://doi.org/10.1073/pnas.1708288114); pmid: [28808003](https://pubmed.ncbi.nlm.nih.gov/28808003/)
40. H. Zou, Y. Li, X. Liu, X. Wang, An APAF-1-cytochrome c multimeric complex is a functional apoptosome that activates procaspase-9. *J. Biol. Chem.* **274**, 11549–11556 (1999). doi: [10.1074/jbc.274.17.11549](https://doi.org/10.1074/jbc.274.17.11549); pmid: [10206961](https://pubmed.ncbi.nlm.nih.gov/10206961/)
41. A. Bentham, H. Burdett, P. A. Anderson, S. J. Williams, B. Kobe, Animal NLRs provide structural insights into plant NLR function. *Ann. Bot.* **119**, 827–702 (2017). doi: [10.1093/abob/abw024](https://doi.org/10.1093/abob/abw024); pmid: [27562749](https://pubmed.ncbi.nlm.nih.gov/27562749/)
42. J. X. Yue, B. C. Meyers, J. Q. Chen, D. Tian, S. Yang, Tracing the origin and evolutionary history of plant nucleotide-binding site-leucine-rich repeat (NBS-LRR) genes. *New Phytol.* **193**, 1049–1063 (2012). doi: [10.1111/j.1469-8137.2011.04006.x](https://doi.org/10.1111/j.1469-8137.2011.04006.x); pmid: [22212278](https://pubmed.ncbi.nlm.nih.gov/22212278/)
43. A. M. Keestra et al., Manipulation of small Rho GTPases is a pathogen-induced process detected by NOD1. *Nature* **496**, 233–237 (2013). doi: [10.1038/nature12025](https://doi.org/10.1038/nature12025); pmid: [23542589](https://pubmed.ncbi.nlm.nih.gov/23542589/)
44. H. Xu et al., Innate immune sensing of bacterial modifications of Rho GTPases by the PIRIN inflammasome. *Nature* **513**, 237–241 (2014). doi: [10.1038/nature13449](https://doi.org/10.1038/nature13449); pmid: [24919149](https://pubmed.ncbi.nlm.nih.gov/24919149/)
45. J. M. Davies, H. Tsuruta, A. P. May, W. I. Weis, Conformational changes of p97 during nucleotide hydrolysis determined by small-angle x-ray scattering. *Structure* **13**, 183–195 (2005). doi: [10.1016/j.str.2004.11.014](https://doi.org/10.1016/j.str.2004.11.014); pmid: [15698563](https://pubmed.ncbi.nlm.nih.gov/15698563/)
46. Y. Shomura et al., Regulation of Hsp70 function by HspBP1: Structural analysis reveals an alternate mechanism for Hsp70 nucleotide exchange. *Mol. Cell* **17**, 367–379 (2005). doi: [10.1016/j.molcel.2005.08.004](https://doi.org/10.1016/j.molcel.2005.08.004); pmid: [15694338](https://pubmed.ncbi.nlm.nih.gov/15694338/)
47. P. Mestre, D. C. Baulcombe, Elicitor-mediated oligomerization of the tobacco N disease resistance protein. *Plant Cell* **18**, 491–501 (2006). doi: [10.1105/tpc.105.037234](https://doi.org/10.1105/tpc.105.037234); pmid: [16387833](https://pubmed.ncbi.nlm.nih.gov/16387833/)
48. K. J. Schreiber, A. Bentham, S. J. Williams, B. Kobe, B. J. Staskawicz, Multiple domain associations within the Arabidopsis immune receptor RPP1 regulate the activation of programmed cell death. *PLOS Pathog.* **12**, e1005769 (2016). doi: [10.1371/journal.ppat.1005769](https://doi.org/10.1371/journal.ppat.1005769); pmid: [27427964](https://pubmed.ncbi.nlm.nih.gov/27427964/)
49. J. L. Tenthorey et al., The structural basis of flagellin detection by NAIP5: A strategy to limit pathogen immune evasion. *Science* **358**, 888–893 (2017). doi: [10.1126/science.aao1140](https://doi.org/10.1126/science.aao1140); pmid: [29146805](https://pubmed.ncbi.nlm.nih.gov/29146805/)
50. X. Yang et al., Structural basis for specific flagellin recognition by the NLR protein NAIP5. *Cell Res.* **28**, 35–47 (2018). doi: [10.1038/cr.2017.148](https://doi.org/10.1038/cr.2017.148); pmid: [29182158](https://pubmed.ncbi.nlm.nih.gov/29182158/)
51. H. H. Kampinga, E. A. Craig, The HSP70 chaperone machinery: J proteins as drivers of functional specificity. *Nat. Rev. Mol. Cell Biol.* **11**, 579–592 (2010). doi: [10.1038/nrm2941](https://doi.org/10.1038/nrm2941); pmid: [20651708](https://pubmed.ncbi.nlm.nih.gov/20651708/)
52. Jizong Wang et al., Reconstitution and structure of a plant NLR resistosome conferring immunity. *Science* **364**, eaav5870 (2019). doi: [10.1126/science.aav5870](https://doi.org/10.1126/science.aav5870); pmid: [31449474](https://pubmed.ncbi.nlm.nih.gov/31449474/)
53. J. P. Erzberger, J. M. Berger, Evolutionary relationships and structural mechanisms of AAA+ proteins. *Annu. Rev. Biophys. Biomol. Struct.* **35**, 93–114 (2006). doi: [10.1146/annurev.biophys.35.040405.101933](https://doi.org/10.1146/annurev.biophys.35.040405.101933); pmid: [16689629](https://pubmed.ncbi.nlm.nih.gov/16689629/)
54. E. F. Pettersen et al., UCSF Chimera—A visualization system for exploratory research and analysis. *J. Comput. Chem.* **25**, 1605–1612 (2004). doi: [10.1002/jcc.20084](https://doi.org/10.1002/jcc.20084); pmid: [15264254](https://pubmed.ncbi.nlm.nih.gov/15264254/)

ACKNOWLEDGMENTS

We thank J. Lei, X. Li, X. Fan, and H. Wu at Tsinghua University for data collection; Z. Zhou at the Institute of Genetics and Developmental Biology for guiding the isotope assay; and P. Schulze-Lefert at the Max Planck Institute for Plant Breeding Research for critical reading of the manuscript. We acknowledge the Tsinghua University Branch of the China National Center for Protein Sciences (Beijing) for providing the cryo-EM facility support and the computational facility support on the cluster of Bio-Computing Platform. **Funding:** This research was funded by the Strategic Priority Research Program of the Chinese Academy of Sciences (XDB11020200 to J.-M.Z.), the National Natural Science Foundation of China (31421001 to J.C. and 31700660 to Jiz.W.), the Alexander von Humboldt-Foundation (Humboldt Professorship to J.C.), Max Planck-Gesellschaft (Max Planck Fellow to J.C.), the National Key R&D Program of China (grant 2016YFA0501100 to H.-W.W.), the Beijing Municipal Science and Technology Commission (grant Z161100000116034 to H.-W.W.), and the China Postdoctoral Science Foundation (2016M600081 to Jiz.W. and 2017M620746 to Jia.W.).

Author contributions: Conceptualization: J.C., J.-M.Z., and H.-W.W.; methodology: J.C., J.-M.Z., H.-W.W., Jiz.W., and M.H.; investigation: Jiz.W., Jia.W., M.H., and J.Q.; validation: Jiz.W., Jia.W., M.H., and G.W.; supervision: J.C., J.-M.Z., H.-W.W., Y.Q., and Z.H.; writing, original draft: J.C.; writing, review and editing: J.C., J.-M.Z., H.-W.W., Jiz.W., Jia.W., and M.H.; funding acquisition: J.C., J.-M.Z., H.-W.W., and Jiz.W. **Competing interests:** The authors declare no competing interests. **Data and materials availability:** All data needed to replicate the work is present either in the supplementary

materials or in the listed Protein Data Bank files. For the ZAR1-RKS1 complex, the atomic coordinates and EM map have been deposited in the Protein Data Bank and Electron Microscopy Database with accession codes 6J5W and EMD-0683, respectively. For the ZAR1-RKS1-PBL2^{NBD} complex, the atomic coordinates with or without the NBD have been deposited in the Protein Data Bank with accession codes 6J5V and 6J5U, respectively, and the EM maps with or without the NBD have been deposited in the Electron Microscopy Database with accession codes EMD-0682 and EMD-0681, respectively.

SUPPLEMENTARY MATERIALS

www.sciencemag.org/content/364/6435/eaav5868/suppl/DC1

Materials and Methods

Figs. S1 to S11

Table S1

References (55–72)

1 October 2018; accepted 13 February 2019

10.1126/science.aav5868

Ligand-triggered allosteric ADP release primes a plant NLR complex

Jizong Wang, Jia Wang, Meijuan Hu, Shan Wu, Jinfeng Qi, Guoxun Wang, Zhifu Han, Yijun Qi, Ning Gao, Hong-Wei Wang, Jian-Min Zhou and Jijie Chai

Science **364** (6435), eaav5868.
DOI: 10.1126/science.aav5868

The plant resistosome comes into focus

Nucleotide-binding, leucine-rich repeat receptors (NLRs) initiate immune responses when they sense a pathogen-associated effector. In animals, oligomerization of NLRs upon binding their effectors is key to downstream activity, but plant systems differ in many ways and their activation mechanisms have been less clear. In two papers, Wang *et al.* studied the composition and structure of an NLR called ZAR1 in the small mustard plant *Arabidopsis* (see the Perspective by Dangl and Jones). They determined cryo-electron microscopy structures that illustrate differences between inactive and intermediate states. The active, intermediate state of ZAR1 forms a wheel-like pentamer, called the resistosome. In this activated complex, a set of helices come together to form a funnel-shaped structure required for immune responsiveness and association with the plasma membrane.

Science, this issue p. eaav5868, p. eaav5870; see also p. 31

ARTICLE TOOLS

<http://science.sciencemag.org/content/364/6435/eaav5868>

SUPPLEMENTARY MATERIALS

<http://science.sciencemag.org/content/suppl/2019/04/03/364.6435.eaav5868.DC1>

RELATED CONTENT

<http://science.sciencemag.org/content/sci/364/6435/eaav5870.full>
<http://science.sciencemag.org/content/sci/364/6435/31.full>

REFERENCES

This article cites 72 articles, 28 of which you can access for free
<http://science.sciencemag.org/content/364/6435/eaav5868#BIBL>

PERMISSIONS

<http://www.sciencemag.org/help/reprints-and-permissions>

Use of this article is subject to the [Terms of Service](#)